PROCEEDINGS, 44th Workshop on Geothermal Reservoir Engineering
Stanford University, Stanford, California, February 11-13, 2019
SGP-TR-214

Benchmark test and sensitivity analysis for Geothermal Applications in the Netherlands

Yang Wang[1], Mark Khait[1], Denis Voskov[1,2], Sanaz Saeid[1], David Bruhn[1,3]

[1]Delft University of Technology, Stevinweg 1, 2628 CN Delft, Netherlands

[2]Stanford University, CA 94305-4007, USA

[3]Helmholtz Center Potsdam GFZ, Germany

y.wang-18@tudelft.nl

D.V.Voskov@tudelft.nl

Keywords: geothermal simulation, thermal breakthrough, sensitivity analysis in geothermal reservoirs

ABSTRACT

Accurate prediction of temperature and pressure distribution is essential for geothermal reservoir exploitation with cold-water re-injection. Depending on our knowledge about the heterogeneous structure of the subsurface, reservoir development scheme can be optimized, and the overall lifetime of the geothermal field can be extended. In this study, we present Delft Advanced Research Terra Simulator (DARTS) which can provide fast and accurate flow response of the geothermal field. This simulation framework is using the Operator-Based Linearization (OBL) technique and is suitable for uncertainty analysis with a large ensemble of models. In DARTS, we select the molar formulation with pressure and enthalpy as primary variables. In addition, a fully-implicit two-point flux approximation on an unstructured grid is implemented to solve the mass and energy conservation equations. In our work, DARTS is compared with the state-of-the-art simulation frameworks using benchmark tests within synthetic geological models. We demonstrate that our simulator achieved a good match for both low- and high-enthalpy conditions with the maximum spatial difference in pressure and temperature below 2% in comparison to other simulators. At the same time, DARTS provide high performance and flexibility of the code due to OBL approach which makes it particularly useful for uncertainty quantification. We investigated the influence of different geological parameters to the thermal breakthrough time for both low- and high-enthalpy conditions and found that the system lifetime heavily relies on variation in hydrothermal reservoir properties. Afterward, we conducted a series of sensitivity analysis for various production regimes and geological properties in realistic geothermal case studies.

1. INTRODUCTION

Geothermal energy has attracted attention as a kind of renewable energy for several decades. However, the uncertainty in geothermal reservoir development can directly impact the technical and economic feasibility of geothermal projects. The lifecycle and heat recovery often vary a lot with both formation statistics and production management.

Numerical simulation, as a powerful and predictive tool, has been widely used for uncertainty analysis and optimization. Several simulators have been used in geothermal applications (O'Sullivan et al., 2001). However, the complexity of the physics and a large number of grid blocks in high-resolution geothermal models often challenge the conventional simulation techniques. The complex physical processes (i.e. multi-phase flow, multi-component reactive transport) often encountered in geothermal applications require robust, flexible and efficient solutions. In addition, large models with multi-million control volumes are often needed to characterize and predict the behavior of geothermal reservoir which slows down the simulation process. Furthermore, in order to quantify uncertainties and optimize development strategies, a large ensemble of models are necessary to cover the wide range of parameter settings, which requires high-performance and reliability of forward simulations.

In this work, we present Delft Advanced Research Terra Simulator (DARTS) developed for various industrial applications including geothermal reservoir modeling (DARTS, 2019). DARTS is based on the Operator-based Linearization (OBL) framework, which has been proposed recently for complex multiphase flow and transport applications and aims to improve the simulation performance (Voskov, 2017; Khait and Voskov, 2018a).

In the OBL approach, the mass and energy conservation equations are written in the summative form, where each term is split into the product of two operators depending on spatial properties and physical state respectively. The space-dependent operators are treated in conventional way. The state-dependent operators are represented in an approximate form using physical supporting points and multilinear interpolation between them. This representation simplifies the construction of the Jacobian matrix and residuals since the complex physics is translated into generic interpolation calculated in an adaptive way (Khait and Voskov, 2018b). As a result, the programming code is significantly simplified with enough flexibility and high performance. Furthermore, the architecture of the code supports farther extension to parallel computation and GPU programming (Khait and Voskov, 2017).

In this paper, we briefly introduce the basics of the OBL approach used in DARTS. Next, a set of benchmark tests is conducted, and the results are compared with TOUGH2 (Pruess et al., 1999) and ADGPRS (Automatic-Differentiation General Purpose Research Simulator) (Garipov et al., 2018). After the validation, a series of sensitivity tests are performed for a realistic geothermal field. This sensitivity analysis can provide guidance and instruction for future geothermal field operations in the presence of physical uncertainties.

2. METHODOLOGY

Here, we consider the governing equations and nonlinear formulation for two-phase thermal simulation with aqueous brine. This problem can be described by mass and energy equations:

$$\frac{\partial}{\partial t}\left(\phi \sum_{j=1}^{n_p} \rho_j s_j\right) - div \sum_{j=1}^{n_p} \rho_j u_j + \sum_{j=1}^{n_p} \rho_j \tilde{q_j} = 0, \tag{1}$$

$$\frac{\partial}{\partial t}(\phi \sum_{j=1}^{n_p} \rho_j s_j U_j + (1-\phi)U_r) - div \sum_{j=1}^{n_p} h_j \rho_j u_j + div(\kappa \nabla T) + \sum_{j=1}^{n_p} h_j \rho_j \tilde{q_j} = 0, \tag{2}$$

where: ϕ is porosity, s_j is phase saturation, ρ_j is phase molar density, U_j is phase internal energy, U_r is rock internal energy, h_j is phase enthalpy, κ is thermal conduction.

The saturation constraint requires:

$$\sum_{j=1}^{n_p} s_j = 1. \tag{3}$$

In addition, Darcy's law is used to describe the fluid flow in the reservoir,

$$u_j = K \frac{k_{rj}}{\mu_j}\left(\nabla p_j - \gamma_j \nabla D\right), \tag{4}$$

where: K is permeability tensor, k_{rj} is relative permeability, μ_j is phase viscosity, p_j is pressure in phase j, γ_j is gravity vector, D is depth.

Molar formulation (Faust and Mercer, 1975; Wong et al., 2015) was taken as the system nonlinear formulation, in which pressure and enthalpy were chosen as primary variables. As conventional linearization approach of the nonlinear equation system, the Newton-Raphson method is adopted to solve the linearized system of equations on each nonlinear iteration in the following form:

$$J(\omega^k)(\omega^{k+1} - \omega^k) + r(\omega^k) = 0, \tag{5}$$

where J is the Jacobian defined at the k_{th} nonlinear iteration. Conventional linearization approach requires the Jacobian assembly with accurate numerical property values and their derivatives with respect to nonlinear unknowns. This may demand either various interpolations (for properties such as relative permeabilities) or solution of a highly nonlinear system in combination with chain rule and inverse theorem (Voskov and Tchelepi, 2012). As a result, the nonlinear solver has to resolve all small variations in property descriptions, which are sometimes unimportant due to the numerical nature and uncertainties in property evaluation. Next, we present the Operator-Based linearization approach which helps to improve this behavior.

3. OPERATOR-BASED LINEARIZATION (OBL)

Following the OBL approach, all variables in the Eqs. (1) and (2), excluding the ones from the phase source term, are expressed as functions of a physical state ω and/or a spatial coordinate ξ.

Pressure and enthalpy are taken as the unified state variables of a given control volume. Flux-related fluid properties are defined by the physical state of upstream block ω_{up}, determined at interface l. The state-dependent operator is defined as a function of the physical state only; the space-dependent operator is defined by both physical state ω and spatial coordinate ξ. The discretized mass conservation equation in operator form reads:

$$a(\xi,\omega)(\alpha(\omega) - \alpha(\omega_n)) + \sum_l b(\xi,\omega)\beta(\omega) + \theta(\xi,\omega,u) = 0, \tag{6}$$

$$a(\xi,\omega) = \phi V, \alpha(\omega) = \sum_{j=1}^{n_p} \rho_j s_j, b(\xi,\omega) = \Delta t \Gamma^l \Phi_{p,ij}, \beta(\omega) = \sum_{j=1}^{n_p} \rho_j^l \frac{k_{rj}^l}{\mu_j^l}, \tag{7}$$

$$\Phi_{p,ij} = \left(p_j + \gamma_p(\omega_j) - p_i - \gamma_p(\omega) - \frac{\delta_p(\omega) + \delta_p(\omega_j)}{2}(D_j - D_i)\right), \tag{8}$$

where, ω_n is the physical state of block i in the previous timestep, ω_j is the physical state of block j, $\gamma_p(\omega)$ is the capillary pressure operator for phase p, $\delta_p(\omega)$ is the density operator for phase p.

The discretized energy conservation equation in operator form is as follows:

$$a_e(\xi,\omega)(\alpha_e(\omega)-\alpha_e(\omega_n))+\sum_l b_e(\xi,\omega)\beta_e(\omega)+\sum_l c_e(\xi,\omega)\gamma_e(\omega)+\theta_e(\xi,\omega,u)=0, \tag{9}$$

$$a_e(\xi)=V(\xi),\qquad \alpha_e(\omega)=\phi\left(\sum_{j=1}^{n_p}\rho_j s_j U_j-U_r\right)+U_r, b_e(\xi,\omega)=b(\xi,\omega), \beta_e(\omega)=\sum_{j=1}^{n_p} h_j^l \rho_j^l \frac{k_{rj}^l}{\mu_j^l}, \tag{10}$$

$$c_e(\xi)=\Delta t\Gamma^l(T^b-T^a);\ \gamma_e(\omega)=\phi\left(\sum_{j=1}^{n_p} s_j\lambda_j-\kappa_r\right)+\kappa_r. \tag{11}$$

This representation simplifies complicated nonlinear physics significantly. Instead of performing complex evaluations of properties and their derivatives with respect to nonlinear unknowns during the simulation, we can parameterize operators in physical space at the pre-processing stage or adaptively with a limited number of supporting points. The evaluation of operators during the simulation is based on multilinear interpolation, which improves the performance of the linearization stage. In addition, due to the piece-wise representation of operators, the nonlinearity of the system is reduced which improves the nonlinear behaviour (Khait and Voskov, 2018 a,b).

4. BENCHMARK TEST

In this section, we perform a series of benchmark tests using DARTS in a synthetic geothermal model and compare the simulation results with TOUGH2 and ADGPRS. First, we describe the geothermal model used in the benchmark. Next, we compare simulation results of geothermal heat production for both low- and high-enthalpy conditions. Finally, we display the performance of different simulators.

4.1 Three-dimensional geothermal model

A synthetic geological model (Willems et al., 2016; Shetty et al., 2018) is constructed based on typical geology of the West Netherlands Basin (WNB), a 60-km-wide basin in the southwest of the Netherlands (Donselaar et al., 2015). This model is used for benchmark tests. All properties in the model are populated based on the dataset of the fluvial Nieuwerkerk Formation of the WNB (Willems et al., 2017).

The reservoir dimensions are 1.8km×1.2km×0.1km as shown in Figure 1. The discretized model contains 60×40×42 grid-blocks. The well doublet is placed in the middle of the model, along the X-axis with a spacing of 0.99km. The fluvial sandstone bodies are located along the longer side of the reservoir, with the porosity distributed within the range [0.16, 0.36] and permeability distributed within the range [6, 3360] mD. The boundary conditions along the short (X-axis) of the reservoir are set to a constant initial pressure; the boundary conditions at the other sides are set to no flow. Two energy-transfer mechanisms are involved in this process: convective and conductive heat flow.

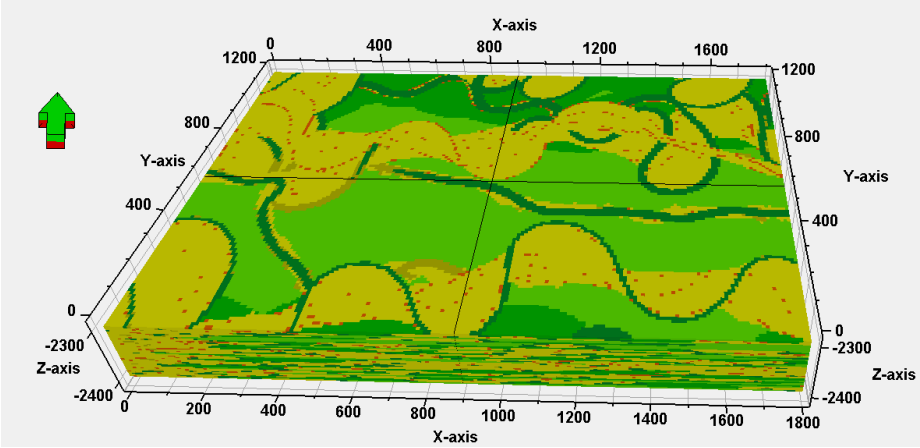

Figure 1: Schematic of the facies distribution for synthetic geothermal model

4.2 Results comparison

In the comparison study, because of the complexity of data pre-processing in TOUGH2 and some convergence issues in ADGPRS for the high-enthalpy condition, the top layer of the model is used to run and compare under low- and high-enthalpy condition within 3 simulators. The full model is only compared with ADGPRS under low-enthalpy condition.

4.2.1 Comparisons of DARTS and TOUGH2

Table 1 shows the initial conditions and well controls. The results are shown in Figure 2 and 3 for low- and high-enthalpy respectively. TOUGH2 solution is taken as the reference. A good match can be observed between DARTS and TOUGH2 results under both

conditions. The maximum relative temperature error is around 1%. Notice that in both simulators, the IAPWS-IF97 of the International Association for the Properties of Water and Steam is used to calculate the fluid properties.

Table 1: Different conditions and well controls for tests with TOUGH2

	Low-enthalpy condition	High-enthalpy condition
Initial temperature (K)	348.15	498.15
Initial pressure (bar)	200	
Injection enthalpy (kJ/kg)	100	
Injection rate (m^3/day)	36	
Production rate (m^3/day)	36	

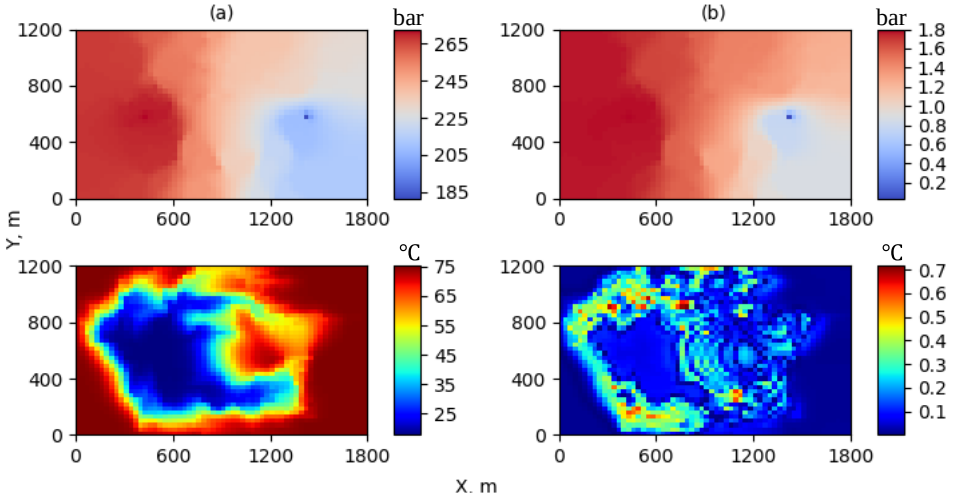

Figure 2: Left: pressure (top) and temperature (bottom) profiles from TOUGH2 for low-enthalpy condition after 100 years. Right: absolute error between TOUGH2 and DARTS for pressure (top) and temperature (bottom).

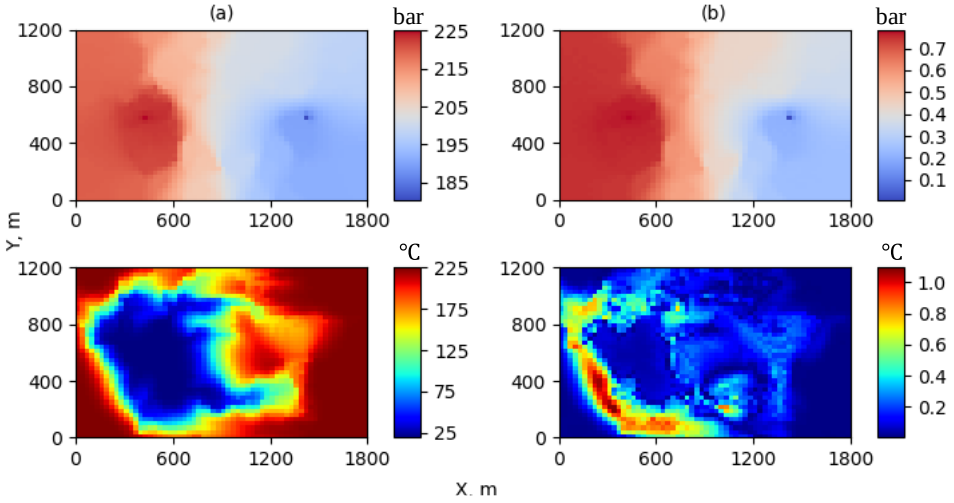

Figure 3: Left: pressure (top) and temperature (bottom) profiles from TOUGH2 for high-enthalpy condition after 100 years. Right: absolute error between TOUGH2 and DARTS for pressure (top) and temperature (bottom).

4.2.2 Comparison of DARTS and ADGPRS

Here, we take ADGRPS solution as the reference. Figure 4 and 5 shows the solution and error of single-layer model. Figure 6 shows the solution and error of 3 layers in the full model.

As shown in Figure 4, for single-layer model under low-enthalpy condition, the maximum temperature difference between DARTS and ADGPRS is 1.4℃, which is around 3% of the overall temperature variation range. For the high-enthalpy case (Figure 5), the temperature range is 25 to 225℃. The maximum temperature difference of 3.5℃ is within 2% of the overall temperature difference. In

Figure 6, the maximum temperature error is around 1.2℃ for full-layer model under low-enthalpy condition, which shows good match as well. Please note that fluid property models are different in DARTS and ADGPRS (see Wong et al., 2015 for details).

Table 2 Different conditions and well controls for tests with ADGPRS

	Low-enthalpy condition	High-enthalpy condition
Initial temperature (K)	348.15	498.15
Initial pressure (bar)	200	200
Injection temperature (K)	298.15	298.15
Injection rate (m^3/day)	2400	60
Production rate (m^3/day)	2400	60

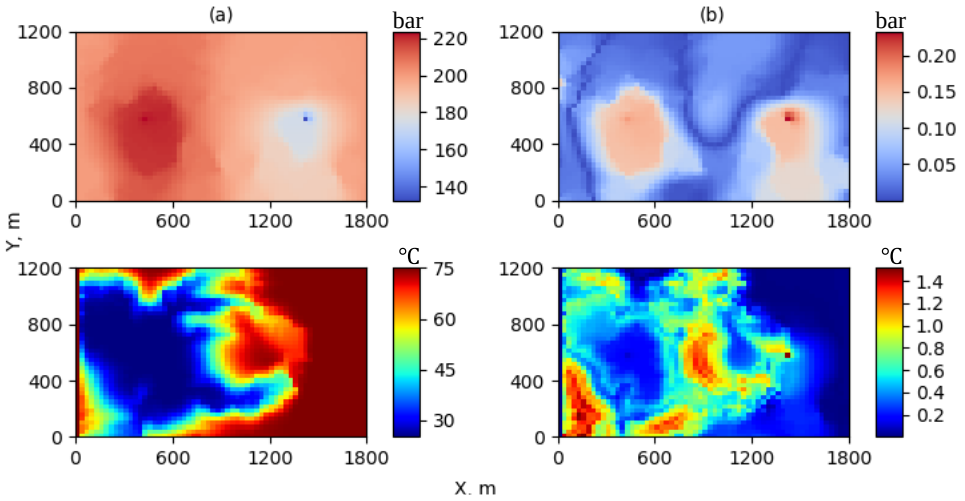

Figure 4: Left: pressure (top) and temperature (bottom) profiles from ADGPRS for low-enthalpy condition after 100 years. Right: absolute error between ADGPRS and DARTS for pressure (top) and temperature (bottom).

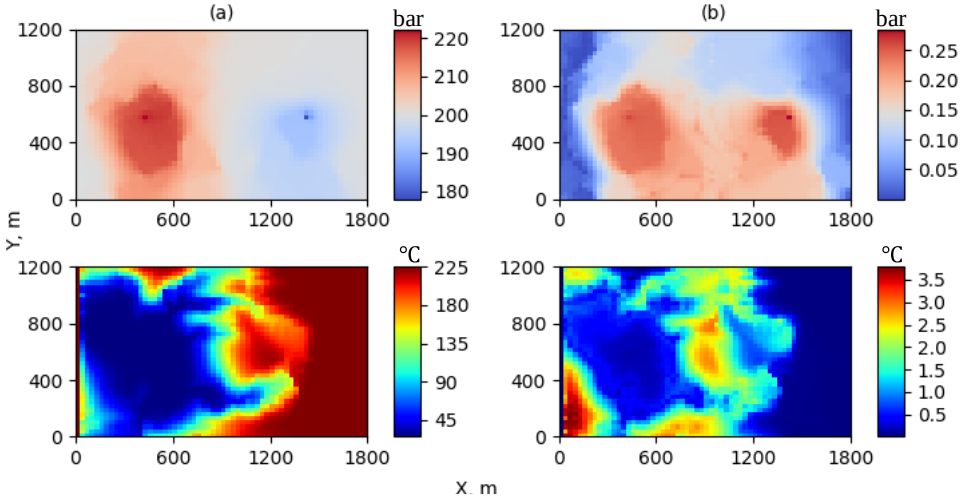

Figure 5: Left: pressure (top) and temperature (bottom) profiles from ADGPRS for high-enthalpy condition after 100 years. Right: absolute error between ADGPRS and DARTS for pressure (top) and temperature (bottom).

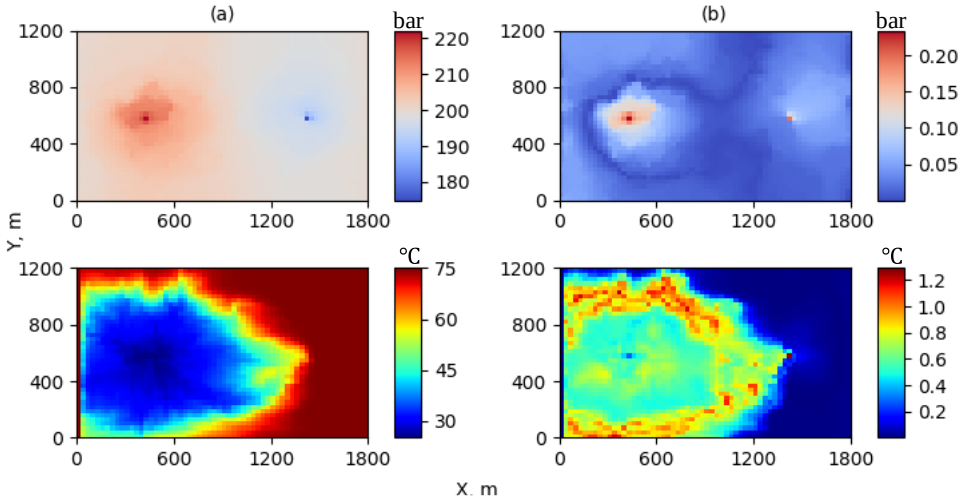

(i) 1st layer

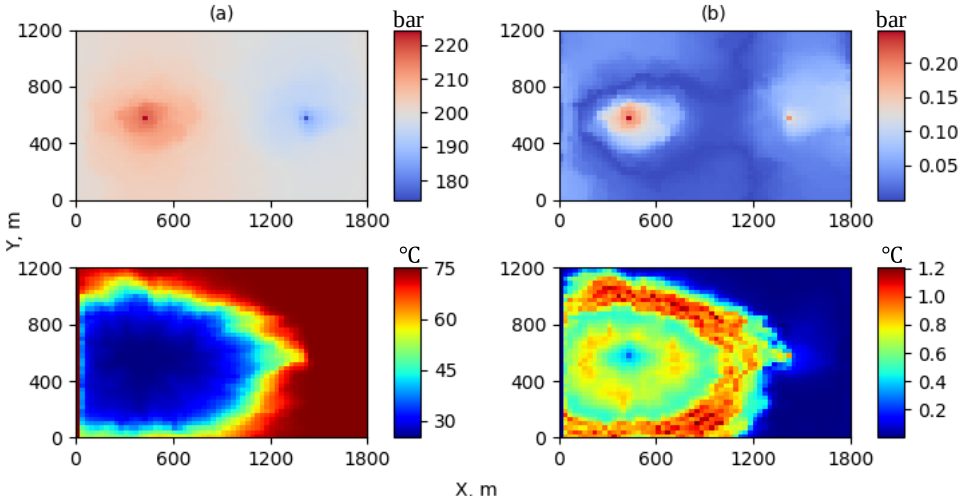

(ii) 20th layer

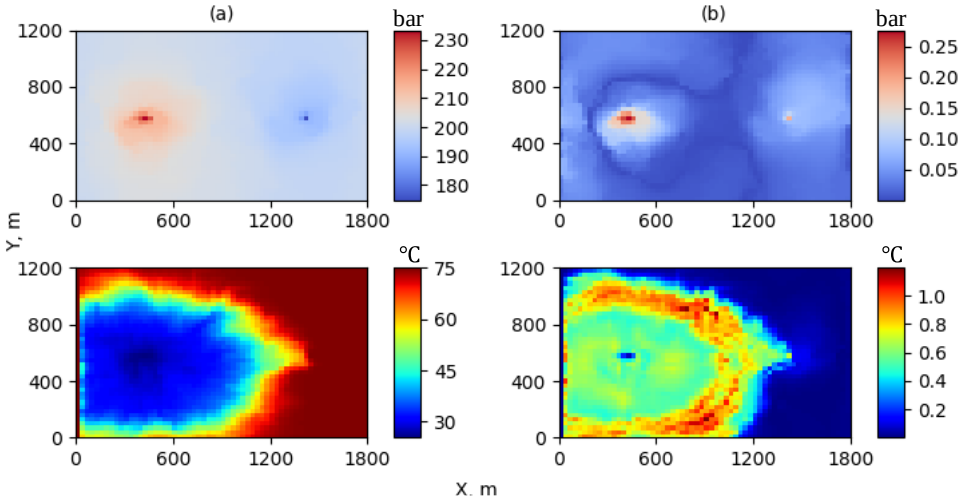

(iii) 40th layer

Figure 6: Results of 3 selected layers from the full-model comparison under low-enthalpy condition after 100 years. Left: pressure (top) and temperature (bottom) profiles of ADGPRS. Right: pressure (top) and temperature (bottom) profiles of DARTS-ADGRPS absolute error.

4.2.3 Performance comparison

Table 3 shows the performance of different simulators on the same desktop Intel(R) Xeon(R) CPU 3.50GHz. All runs have been performed in single thread regime. It is clear that DARTS achieves a better performance than TOUGH2 and ADGPRS among these runs. A small timestep of 20 days is needed in the first four runs for DARTS to match converged simulation timesteps in TOUGH2. Since the timestep control in DARTS is different from TOUGH2, there is a slight difference in the total number of timesteps. The fast simulation in DARTS can be attributed to the OBL approach, which significantly simplifies the calculation of state-dependent properties and Jacobian assembly. A slightly higher number of nonlinear iterations in DARTS runs in comparison to ADGPRS in low enthalpy cases is related to different convergence criteria.

Table 3: Comparison of simulation parameters for 100 years among different simulators

Test case	Simulator	Target timestep (day)	Number of timesteps	Nonlinear iteration	Linear iteration	CPU time (s)
Low-enthalpy top layer model	DARTS	20	1835	3720	36000	34.6
	TOUGH2	20	1935	--	--	403
High-enthalpy top layer model	DARTS	20	1835	3861	37963	38.7
	TOUGH2	20	2118	--	--	429
Low-enthalpy top layer model	DARTS	365	115	259	1950	2.9
	ADGPRS	365	115	253	1616	14.8
High-enthalpy top layer model	DARTS	365	115	287	2286	3.4
	ADGPRS	365	115	378	3396	18.2
Low-enthalpy full model (42 layers)	DARTS	365	115	242	2997	159.3
	ADGPRS	365	115	264	2437	446

5. SENSITIVITY STUDY USING A REALISTIC GEOTHERMAL RESERVOIR

Based on the benchmark study with different simulators described above, we have verified the accuracy of simulation in DARTS. Since the lifetime of a geothermal project is impacted by both formation statics and well management, the sensitivity analysis is necessary to optimize the development scheme, extend the lifetime and improve the economic feasibility of the geothermal reservoir. In this section, we conduct a sensitivity analysis using a realistic model of a highly-heterogeneous geothermal field in the Netherlands.

5.1 Reservoir description

The research area is located in the West Netherlands Basin, which is an inverted rift basin. Sediments in this basin range in age from Jurassic to recent and are overlying Triassic and older sediments. The Upper Jurassic and Lower Cretaceous start with the continental sediments of the Nieuwerkerk Formation. These sediments were deposited in subsiding half-grabens, while adjacent highs were subjected to erosion.

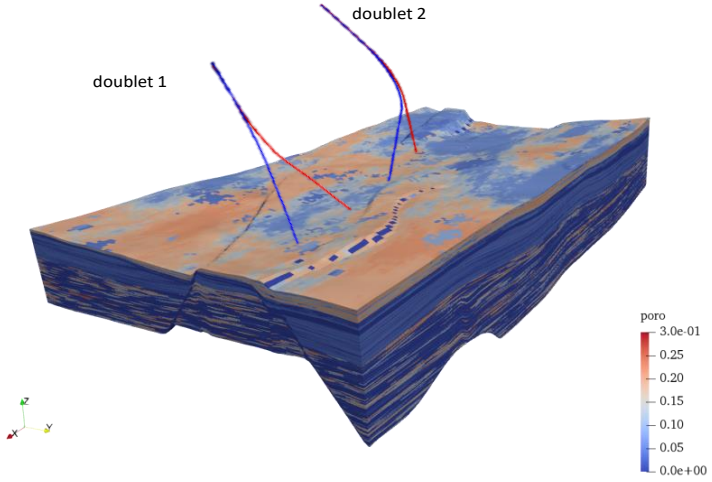

Figure 7: Porosity distribution of the geothermal reservoir for sensitivity analysis. In this figure, injection wells are shown by blue and production wells by red.

In the Nieuwerkerk Formation, the Delft Sandstone has in general good reservoir properties. The Delft Sandstone is interpreted to be deposited as stacked distributary-channel deposits in a lower coastal plain setting resulting in massive sandstone sequences. The thickness of the Delft Sandstone is influenced by the syn-rift deposition of the sediments and therefore the Delft Sandstone is of variable thickness, a thickness up to 130m is observed. The sandstone consists of fine- to coarse-grained sand, the lateral continuity is difficult to predict. The Berkel Sandstone Member and Berkel Sands-Claystone Member have a shallow marine depositional setting. The facies range from upper shoreface to lower shoreface of a coastal-barrier system. Lateral continuity is often good and cementation low. The permeability of the sands is good to excellent ranging from 400 to >3,000 mD. Porosities range from 20 to 30%.

5.2 Numerical model description and sensitivity analysis

- The grid dimension is 177×85×895.
- No flow boundary condition is defined to run the simulation.
- The initial condition of the reservoir is 200bar, 348.15K.
- Two doublets exist in the model; doublet 1 works with rate control and doublet 2 works under bottom hole pressure control. Injection temperature is 308.15K.
- For the correlation between permeability and porosity, two sets of relationship are taken: one (Model1) is from the service company with this geothermal project; the other one (Model2) is from the correlation for Berkel, Rijswijk and Delft Sandstones.
- When the cold front arrives at the production well, temperature drops below a certain limit (338K in this study) and the doublet lifetime is reached.

5.2.1 Base case

Table 4 gives the basic parameter settings for the reference model. Next, we change some of these parameters and observe the changes in production temperature of both doublets.

Table 4 Parameters for base case test

Doublet 1		Doublet 2		Parameter	Value
Well name	Rate control (m^3/day)	Well name	BHP control (bar)	k_v/k_h	0.1
I1	4800	I2	230	K~ϕ	Model1
P1	4800	P2	180	Fault	Sealed

5.2.2 Vertical and horizontal permeability ratio

The permeability ratio between vertical and horizontal directions can impact the direction of fluid flow, which in turn influences the thermal propagation. Here, the permeability ratio is chosen with 3 values: k_v/k_h=0.01,0.1,1.

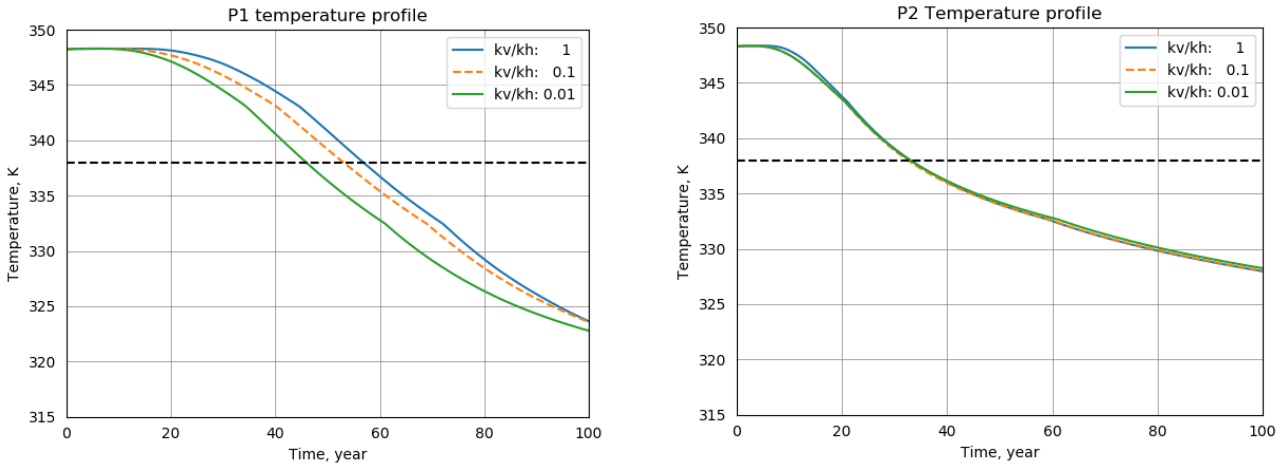

(a) (b)

Figure 8: Temperature change of P1 and P2 for different vertical and horizontal permeability ratio

As shown in Figure 8(a), the lifetime of doublet 1 is quite sensitive to the changes in permeability ratio. With the increase in vertical permeability, the lifetime is extended, which means there is more heat swept with a similar vertical and horizontal permeability. On the other hand, for a low permeability ratio, the interlayer communication is bad and heat sweep efficiency is lower. In Figure 8(b), the lifetime of doublet 2 is insensitive to the permeability ratio. This can be attributed to the fact that this doublet is drilled through multiple impermeable interlayers, which already separates the fluid flow in vertical direction.

5.2.3 Production rate

The injector and producer (I1 and P1) in doublet 1 are set with rate control and we try to observe the temperature change with time at the production well by adjusting well controls. For doublet 2, both wells (I2 and P2) are set with bottom hole pressure (BHP) control and the well conditions stay the same. Figure 9 (a) and (b) show the temperature change of P1 and P2. We can see the temperature profile of P1 varies a lot with the rate variation at both injector (I1) and producer (P1), while there seems no change on the temperature profile of P2 because of its constant BHP well settings and limited communication with the first doublet.

Table 5 Well control setting of both doublets

Well name	Rate control (m^3/day)			BHP control (bar)
I1	2400	4800	7200	--
P1	2400	4800	7200	--
I2	--			230
P2	--			180

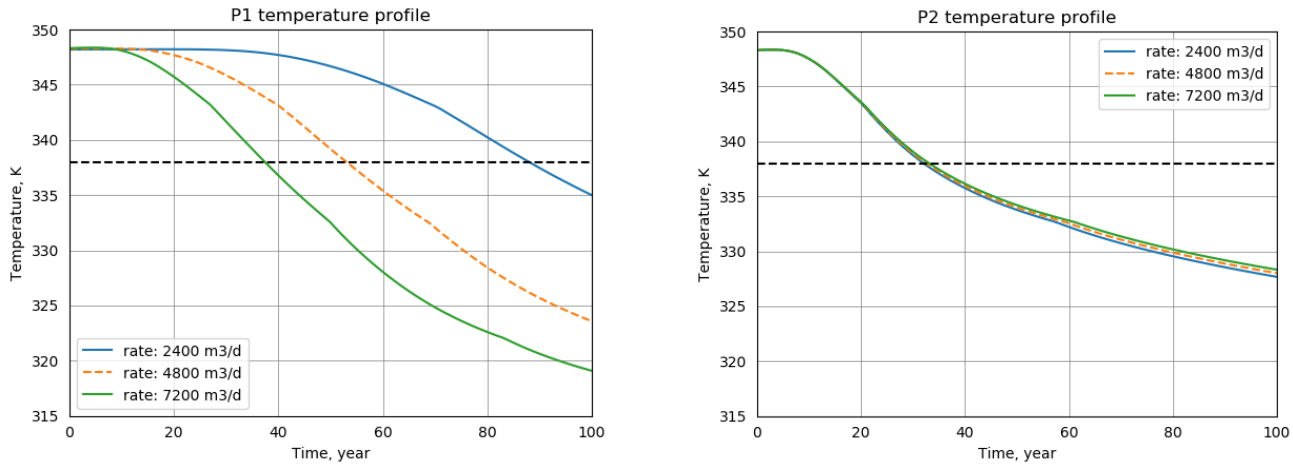

(a) **(b)**

Figure 9: Temperature change of production wells (P1 and P2) under different production rate

5.2.4 Fault connectivity

In Figure 10, there is a fault along the direction of doublet distribution. Through setting the fault as impermeable (or sealed) and permeable, we observe the influence of fault connectivity to temperature propagation. The two doublets are on the same side of the fault. Simulation results show very low sensitivity of fault permeability to the thermal breakthrough time of the doublets. This is because the fluid flow will not go across the faults and heat propagation moves towards producer directly. However, we can still see the difference in enthalpy profile with different fault connectivity. In Figure 10 (a), since the fault is fully sealed, the cold front will only propagate by heat conduction when it reaches the fault. In Figure 10(b), the fault is permeable and the cold front can move across by both fluid convection and heat conduction. Therefore, if we have wells on different sides of the fault, the fault connectivity will impact the behaviour and the lifetime of the doublets.

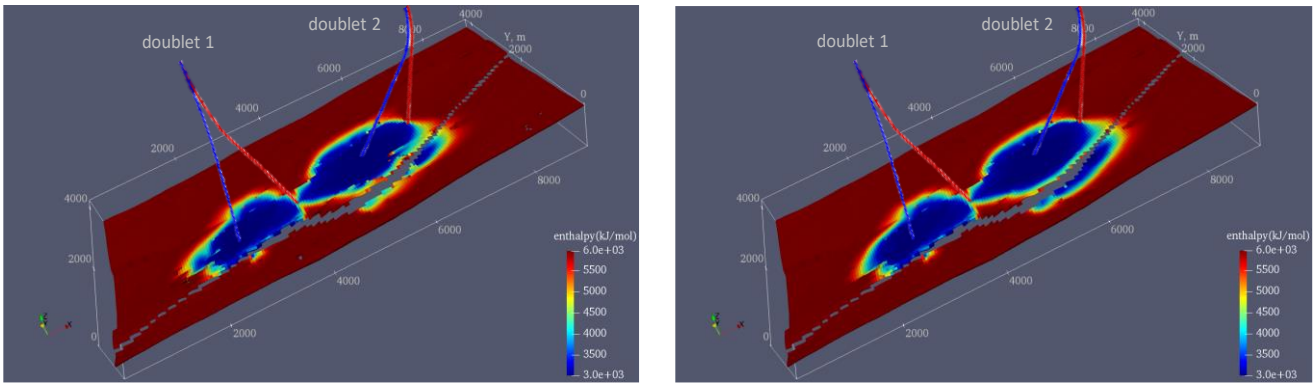

(a) **(b)**

Figure 10: Enthalpy profile with different fault connectivity after 100 years of operation

5.2.5 Permeability-porosity correlation

The relationship between permeability and porosity is another source of uncertainties in the geothermal reservoir. Here we use two different permeability-porosity correlations and try to observe their impact to the production temperature. As shown in Figure 11 (a) and (b), temperature profile changes when correlation is changing but the impact on the lifetime of two doublets is different.

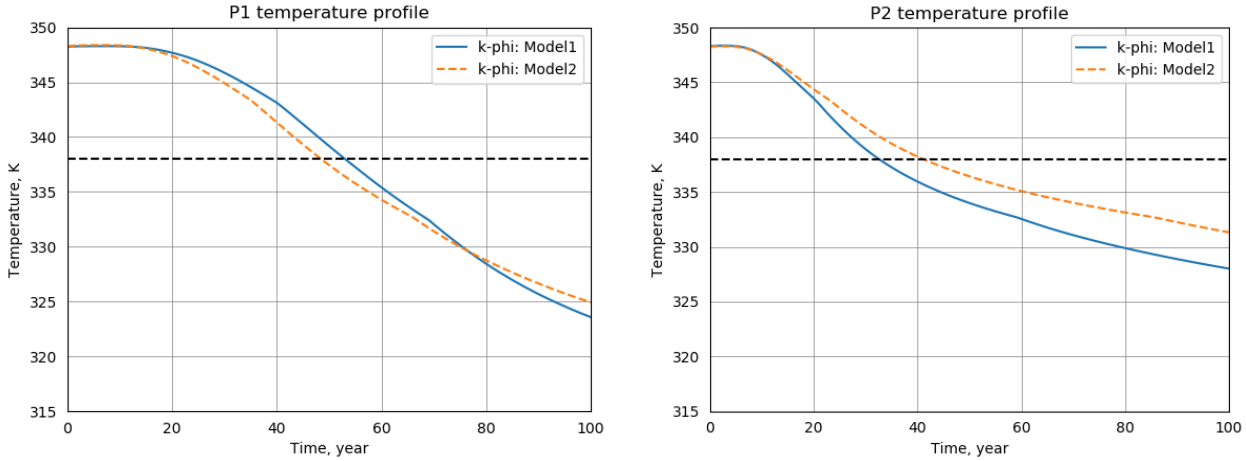

(a) **(b)**

Figure 11: Production temperature of P1 and P2 under different permeability-porosity correlations

CONCLUSION

As a powerful tool, numerical simulation has been widely used for geothermal development. In this paper, we present Delft Advanced Research Terra Simulator (DARTS) which can be used for the prediction of heat production in geothermal projects. DARTS is constructed within the framework of Operator-base Linearization (OBL) approach, which provides advanced flexibility and efficiency. Benchmark tests are conducted within DARTS using synthetic geothermal model in comparison with TOUGH2 and ADGPRS under low- and high-enthalpy conditions. The results show that DARTS achieves good match with the other two simulators, while simulation time is significantly reduced. After validation, we perform sensitivity study using a realistic heterogeneous reservoir located in the South Netherlands. The sensitivity analyses involve both well management and formation statics (permeability ratio, fault connectivity and permeability-porosity correlation). The preliminary results can be used to guide operations in field and perform farther uncertainty quantification studies.

REFERENCES

Collins, D.A., Nghiem, L.X., Li, Y.K. and Grabonstotter, J.E.: An efficient approach to adaptive-implicit compositional simulation with an equation of state. *SPE reservoir engineering*, 1992.

DARTS: Delft Advanced Research Terra Simulator. In *https://darts-web.github.io/darts-web/*, 2019.

Donselaar, M.E., Groenenberg, R.M. and Gilding, D.T.: Reservoir geology and geothermal potential of the Delft Sandstone Member in the West Netherlands Basin. In *Proceedings World Geothermal Congress, 2015*.

Faust, C. R. and Mercer, J. W.: Summary of Our Research in Geothermal Reservoir Simulation. Proceedings. In *Workshop on Geothermal Reservoir Engineering, Stanford University, Stanford*, 1975.

Garipov, T.T., Tomin, P., Rin, R., Voskov, D.V. and Tchelepi, H.A.: Unified thermo-compositional-mechanical framework for reservoir simulation. *Computational Geosciences*, 2018.

Khait, M. and Voskov, D.: GPU-offloaded general-purpose simulator for multiphase flow in porous media. *SPE Reservoir Simulation Conference*, 2017.

Khait, M. and Voskov, D.: Operator-based linearization for efficient modeling of geothermal processes. *Geothermics*, 2018a.

Khait, M. and Voskov, D.: Adaptive Parameterization for Solving of Thermal/Compositional Nonlinear Flow and Transport With Buoyancy. *SPE Journal*, 2018b.

O'Sullivan, M.J., Pruess, K. and Lippmann, M.J.: State of the art of geothermal reservoir simulation. *Geothermics*, 2001.

Pruess, K., Oldenburg, C.M. and Moridis, G.J.: TOUGH2 USER'S GUIDE. 1999.

Shetty, S., Voskov, D. and Bruhn, D.: Numerical Strategy for Uncertainty Quantification in Low Enthalpy Geothermal Projects. In *43rd Workshop on Geothermal Reservoir Engineering, Stanford*, 2018.

Voskov, D.V. and Tchelepi, H.A.: Comparison of nonlinear formulations for two-phase multi-component EoS based simulation. *Journal of Petroleum Science and Engineering*, 2012.

Voskov, D.: Operator-based linearization approach for modeling of multiphase multi-component flow in porous media. *Journal of Computational Physics*, 2017.

Voskov, D. and Zhou, Y.: AD-GPRS Stanford University's Automatic Differentiation based General Purpose Research Simulator user manual. website: http://pangea.stanford.edu/researchgroups/supri-b/.

Wagner, W. and Kretzschmar, H.J.: International Steam Tables-Properties of Water and Steam based on the Industrial Formulation IAPWS-IF97. *Springer Science & Business Media*, 2007.

Willems, C.J.L., Goense, T., Nick, H.M. and Bruhn, D.F.: The relation between well spacing and Net Present Value in fluvial Hot Sedimentary Aquifer geothermal doublets; a West Netherlands Basin case study. In *41st Workshop on Geothermal Reservoir Engineering, Stanford*, 2016.

Willems, C.J.L.: Doublet deployment strategies for geothermal Hot Sedimentary Aquifer exploitation. *Ph.D Thesis*, 2017.

Wong, Z.Y., Horne, R., Voskov, D.: A Geothermal Reservoir Simulator in AD-GPRS. In *Proceedings World Geothermal Congress*, 2015.